

MgO 基外延 BiFeO₃ 薄膜的结构和铁电光伏性能

霍幸民, 张宪贵, 刘立芳, 侯志青, 赵彬, 王云明,
魏东蕊, 董磊, 曾浩宇, 宋建民

(河北农业大学 理学院, 河北 保定 071001)

摘要: **目的** 深入研究 BiFeO₃(BFO)薄膜的结晶结构、生长取向及测试温度对其介电和铁电光伏性能的影响。**方法** 采用偏轴磁控溅射法, 分别以单晶(001)MgO 基片和外延 La_{0.5}Sr_{0.5}CoO₃ (LSCO) 薄膜作为衬底与底电极, 构架 Pt/BFO/LSCO/MgO 异质结构的铁电电容器。采用 XRD 衍射仪表征 LSCO 和 BFO 薄膜的结构与生长取向, 探究 Pt/BFO/LSCO/MgO 异质结构电容器的介电和铁电光伏性能, 重点研究测试温度对其性能的综合影响。**结果** X 射线衍射 (XRD) 和 Phi 扫描结果表明, MgO 基 BFO 与 LSCO 薄膜均为结晶良好的钙钛矿结构, 且满足(001)取向的外延生长。不同电压和频率下的介电测试表明, BFO 铁电薄膜具有较强的铁电性, 正负矫顽电压分别为 3.36、-1.12 V, 但存在明显的介电色散现象, 呈现先减小、后增大的趋势。在~100 kHz 时, 介电损耗最小, 为 0.016; 在 8 MHz 时, 增加到了 0.212。这主要由于不同频率下各种类型电荷的弛豫竞争机制所致。光伏性能测试表明, 在室温 (20 °C)、光强 250 mW/cm² 紫光垂直照射下, 开路电压 (V_{OC}) 和短路电流 (J_{SC}) 分别为 0.32 V 和 0.21 mA/cm²。进一步提高测试温度 (分别为 40、60、80、100 °C) 发现, BFO 铁电薄膜 V_{OC} 呈先缓慢、后快速减小, 而 J_{SC} 呈先快速上升、后下降的趋势, 并在临界温度 80 °C 处展现了更快的光伏响应速度, V_{OC} 和 J_{SC} 分别为 0.30 V 和 0.96 mA/cm²。能带分析表明, 底电极 LSCO 与上电极 Pt 间大的功函数差 (~1 eV) 使得 BFO 薄膜中存在较强的内建电场, 这有利于分离光生载流子, 从而极大提高了 BFO 薄膜的铁电光伏效应。**结论** BFO 是一种具有重要潜在应用价值的优良环保光伏候选材料, 提供了一种提高 BFO 铁电光伏器件性能的切实可行策略。

关键词: 外延薄膜; BiFeO₃; 磁控溅射; 铁电光伏

中图分类号: O484 **文献标识码:** A **文章编号:** 1001-3660(2023)06-0377-07

DOI: 10.16490/j.cnki.issn.1001-3660.2023.06.034

收稿日期: 2022-03-27; 修订日期: 2022-08-31

Received: 2022-03-27; Revised: 2022-08-31

基金项目: 河北农业大学自主培养博士科研启动经费 (PY201809, PY2021005, PY2021012); 河北农业大学师生协同项目 (2021-BHXT-20); 河北农业大学创新创业训练计划项目 (S202110086039, 2020259, 2022164)

Fund: Starting Fund for Independent Doctoral Research of Hebei Agricultural University (PY201809, PY2021005, PY2021012); Collaborative Project Between Teachers and Students of Hebei Agricultural University (2021-BHXT-20); Innovation and Entrepreneurship Training Program of Hebei Agricultural University (S202110086039, 2020259, 2022164)

作者简介: 霍幸民 (2000—), 男, 主要研究方向为功能薄膜材料与器件。

Biography: HUO Xing-min (2000-), Male, Research focus: functional thin film materials and devices

通讯作者: 曾浩宇 (1978—), 男, 硕士, 实验师, 主要研究方向功能薄膜材料与器件。

Corresponding author: ZENG Hao-yu (1978-), Male, Master, Research associate, Research focus: functional thin film materials and devices.

通讯作者: 宋建民 (1976—), 男, 博士, 副教授, 主要研究方向功能薄膜材料与器件。

Corresponding author: SONG Jian-min (1976-), Male, Doctor, Associate professor, Research focus: functional thin film materials and devices.

引文格式: 霍幸民, 张宪贵, 刘立芳, 等. MgO 基外延 BiFeO₃ 薄膜的结构和铁电光伏性能[J]. 表面技术, 2023, 52(6): 377-383.

HUO Xing-min, ZHANG Xian-gui, LIU Li-fang, et al. Structure and Ferroelectric Photovoltaic Properties of Epitaxial BiFeO₃ Thin Films on MgO Substrate[J]. Surface Technology, 2023, 52(6): 377-383.

Structure and Ferroelectric Photovoltaic Properties of Epitaxial BiFeO₃ Thin Films on MgO Substrate

HUO Xing-min, ZHANG Xian-gui, LIU Li-fang, HOU Zhi-qing, ZHAO Bin, WANG Yun-ming, WEI Dong-rui, DONG Lei, ZENG Hao-yu, SONG Jian-min

(School of Science, Hebei Agricultural University, Hebei Baoding 071001, China)

ABSTRACT: Bismuth ferrite BiFeO₃ (BFO), a multiferroic material with both ferroelectric and antiferromagnetic properties, has great potential in ferroelectric photovoltaic applications due to its large residual polarization ($\sim 100 \mu\text{C}/\text{cm}^2$), high Curie temperature ($\sim 810^\circ\text{C}$) and suitable band gap ($\sim 2.7 \text{ eV}$). In particular, the thin film structure has more excellent photoelectric conversion efficiency than single crystal and ceramics. In order to deeply investigate crystalline structure, growth orientation, and effect of test temperature on the dielectric and ferroelectric photovoltaic properties of BFO thin films, the Pt/BFO/La_{0.5}Sr_{0.5}CoO₃(LSCO)/MgO heterostructure ferroelectric capacitor was fabricated by employing off-axis magnetron sputtering, in which the single crystal (001) MgO and epitaxial LSCO film were used as substrates and bottom electrodes, respectively. Some important results were obtained as follows. Firstly, the X-ray diffraction (XRD) and Phi scanning results indicated that the MgO based BFO and LSCO films were not only both good crystallized perovskite structure, but also (00l) epitaxial relationships with MgO substrate. Secondly, when tested at different voltages and frequencies, the BFO ferroelectric film exhibited a stronger ferroelectric property, in which the positive and negative coercive voltages were about 3.36 V and -1.12 V, respectively. However, a obvious dielectric dispersion phenomenon was also observed, namely, dielectric loss had a minimum value of 0.016 at $\sim 100 \text{ kHz}$ and increased to 0.212 at 8 MHz, which was mainly due to the relaxation competition mechanism of various types of charges in BFO ferroelectric film. Thirdly, under a vertical 250 mW/cm² purple light at room temperature (20 $^\circ\text{C}$), the photovoltaic performances revealed that the open circuit voltage (V_{OC}) and short circuit current (J_{SC}) were about 0.32 V and 0.21 mA/cm², respectively. By further increasing test temperatures from 40 $^\circ\text{C}$ to 100 $^\circ\text{C}$ with an interval of 20 $^\circ\text{C}$ (40, 60, 80 and 100 $^\circ\text{C}$), it was found that the values of V_{OC} decreased slowly and then rapidly, while the amplitudes of J_{SC} increased rapidly and then decreased. At a critical temperature of 80 $^\circ\text{C}$, the BFO ferroelectric film exhibited a faster photovoltaic response speed, in which the values of V_{OC} and J_{SC} were about 0.30 V and 0.96 mA/cm², respectively. Finally, the energy band analysis was also conducted to study photovoltaic mechanism in BFO ferroelectric film. It was found that a large work function difference ($\sim 1 \text{ eV}$) between the bottom electrode LSCO and the top electrode Pt film resulted in a strong built-in electric field in the BFO film, which was beneficial to the separation of photo-generated carriers, thereby greatly improving the BFO ferroelectric photovoltaic effect of thin films. In all, this study not only shows that BFO is an excellent and environmentally friendly photovoltaic candidate material with great potential application value, and also provides a practical strategy for improving the performance of BFO ferroelectric photovoltaic devices.

KEY WORDS: epitaxial films; BiFeO₃; magnetron sputtering; ferroelectric photovoltaic

兼具铁电性和反铁磁性的多铁材料铁酸铋 BiFeO₃ (BFO) 因具有大的剩余极化强度 ($\sim 100 \mu\text{C}/\text{cm}^2$)、高的居里温度 ($\sim 810^\circ\text{C}$) 和较小的禁带宽度 ($\sim 2.7 \text{ eV}$) 等特性, 使其在铁电光伏应用方面具有巨大的潜力, 特别是用其制造的薄膜结构具有比单晶和陶瓷更优异的光电转换效率, 现已成为了众多科研工作者关注的热点^[1-2]。实验研究表明, 电极/界面、极化、铁电畴、应力等因素都严重影响 BFO 薄膜的光伏 (Photovoltaic, PV) 性能。Lee 等^[3]报道了 BFO 异质结构器件的界面电子能带结构极大地影响其光吸收和电荷输运性质, 从而影响了其 PV 性能。Yang 等^[4]证明了 71 $^\circ$ 畴壁可以增强 BFO 单晶薄膜的 PV 效应。The 等^[5]

发现 BFO 中的 PV 效应是通过一个电势步骤产生的, 该步骤通过 71 $^\circ$ 或 109 $^\circ$ 畴壁获得。此外, Zhang 等^[6]通过改变 LSMO 衬底上外延 BFO 薄膜的面内应力作用, 调制了 BFO 的光学带隙, 进而使光电转化效率显著增强了约 218%。Sharma 等^[7]研究了 Au/BFO/BTO/BFO/BTO/Pt 异质结构的光伏响应特性, 发现 BFO/BTO 界面应力造成高退极化场, 使光生载流子得到有效分离, 从而极大提高了 BFO 薄膜的铁电光伏效应。BFO 材料存在菱形相、单斜相、四方相、三斜相和正交相等多种晶体结构。一般认为, 压应力会产生单斜相, 而拉应变会产生正交相结构^[8-11]。因此, 可以选择不同晶格常数的衬底与其匹配生长, 其有利

于对光伏效应进行调控^[12-14]。在构架 BFO 多功能薄膜器件的过程中, 电极材料的选择尤为关键, 相对于 Au、Ag 和 Pt 等贵金属材料而言, 具有钙钛矿结构的氧化物电极材料 La_{0.5}Sr_{0.5}CoO₃ (LSCO) 具有低的电阻率, 与 BFO 晶格失配度小, 已被广泛应用于多种功能性薄膜器件的制备^[15-17]。然而, 关于以 LSCO 为底电极的 BFO 铁电光伏器件的系统研究鲜有报道。因此, 本文以(001)取向的单晶 MgO 作为衬底, 利用偏轴磁控溅射法制备了 BFO/LSCO/MgO 异质外延结构, 采用 XRD 衍射仪表征了 LSCO 和 BFO 薄膜的结构与生长取向, 探究了 Pt/BFO/LSCO/MgO 异质结构电容器的介电和铁电光伏性能, 重点研究了测试温度对其性能的综合影响。

1 实验

1.1 样品制备

采用磁控溅射法, 制备了 Pt/BFO/LSCO/MgO 异质结构的铁电电容器。制备过程如下: 使用 5 mm×5 mm×0.5 mm 规格的(001)取向氧化镁 (MgO) 单晶基片作为衬底, 先后分别置于超纯丙酮和无水乙醇中, 超声波清洗 10 min, 随后将其快速放入腔体中, 抽真空度至 2.0×10⁻⁴ Pa。采用射频偏轴磁控溅射法在 (001)MgO 基片上外延生长了约为 40 nm 厚的 LSCO 底电极薄膜, 沉积温度和压强分别为 700 °C 和 1.4 Pa, Ar 和 O₂ 流量分别为 75、25 mL/min。然后增加压强至 2 Pa, 温度保持在 700 °C, 在 50 mL/min 的流量的 Ar 气氛中原位外延生长了厚度约 200 nm 的 BFO 薄膜。随后在 101 325 Pa 的 O₂ 氛围中以 5 °C/min 降温速率冷却至室温, 制备了 BFO/LSCO/MgO 异质结构。采用直流磁控溅射法和掩膜技术, 在靶衬间距为 5.5 cm、2 Pa 高纯氩气、50 W 溅射功率工艺条件下, 室温生长了厚度为 60 nm 的 Pt 上电极薄膜, 最终构架了 Pt/BFO/LSCO/MgO 异质结构的铁电电容器。

1.2 样品性能表征

采用 X 射线衍射仪 (XRD, 丹东 TD3700) 对 BFO/LSCO/MgO 异质结构的结晶和生长取向进行表征。利用 LCR 测试仪 (Agilent E4980, 美国; HIOKI IM353, 日本) 和 I-V 测试仪 (Keithley 2601B, 美国) 分别探究了 Pt/BFO/LSCO/MgO 铁电电容器的介电和光伏性能。

2 结果与分析

2.1 BFO/LSCO/MgO 结构与生长取向

为表征异质结构 BFO/LSCO/MgO 的结晶质量, 首先对其进行了 XRD 测试, 2θ 扫描角度范围为 20°~50°, 步宽为 0.02°, 并以衬底 MgO(002)衍射峰

为基准进行归一化处理, 如图 1 所示。

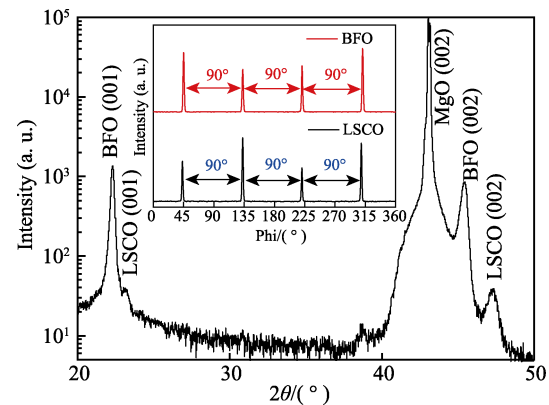


图 1 BFO/LSCO/MgO 异质结构 XRD 和 Phi 图谱
Fig.1 XRD and Phi patterns of BFO/LSCO/MgO heterostructure

由图 1 可知, 除衬底 MgO(002)衍射峰外, 仅出现了 LSCO 和 BFO 薄膜(001)和(002)的特征衍射峰, 且无其他杂相和取向衍射峰出现, 表明 LSCO 和 BFO 薄膜均是结晶质量良好的钙钛矿结构。为进一步探究薄膜生长取向情况, 对薄膜 BFO 的(101)面进行了 Phi 扫描 (如图 1 中插图所示), 发现 BFO 呈现了 4 个相隔均为 90°的衍射峰, 且峰强度基本相同, 表明异质结构满足关系(001)[100]BFO//(001)[100]LSCO//(001)[100]MgO 的外延生长。通过布拉格衍射公式 $2d\sin\theta=n\lambda$ (d 为晶面间距; θ 为入射角; λ 为 X 射线波长, $\lambda=0.154\ 056\ \text{nm}$; n 为正整数) 计算, BFO(001)和 LSCO(001)薄膜的面外晶格常数分别为 0.398 3、0.384 0 nm。不难发现, 二者均大于其相应的块材晶格常数 (分别为~0.396 2 nm 和~0.383 6 nm), 表明 BFO 和 LSCO 薄膜均处于面外拉应变状态。为进一步探究应变产生机制, 此处调研了 BFO、LSCO 和 MgO 的晶格常数和热膨胀系数^[18-22], 见表 1。可以看出, 尽管衬底 MgO 的晶格常数大于 BFO 和 LSCO, 极易在 BFO 和 LSCO 面内产生拉应变, 从而使面外呈压应变状态, 但同时也发现衬底 MgO 的热膨胀系数明显大于 BFO 和 LSCO。因此, 在 BFO 和 LSCO 薄膜生长过程中, 由于与衬底的晶格失配较大, 故随着薄膜厚度的增加, 将产生大量位错以弛豫晶格失配, 同时在降温过程中衬底 MgO 对 BFO 和 LSCO 产生面内压应变。正是基于高温生长过程中的晶格

表 1 BFO/LSCO/MgO 晶格常数和热膨胀系数
Tab.1 Parameters of lattice constants and thermal expansion coefficients of BFO/LSCO/MgO

Materials	Out-of-plane lattice constant of films/nm	Lattice constant of bulks/nm	Out-of-plane strain of films/%	Coefficients of thermal expansion/(10 ⁻⁶ .°C ⁻¹)
BFO	0.398 3	0.396 2	0.5	10.9
LSCO	0.384 0	0.383 6	0.1	10.7
MgO		0.421 1		13.47

失配弛豫和降温过程中的热失配相互竞争作用,且当热失配在此竞争中占主导地位时,最终导致了一定厚度的BFO和LSCO面外呈拉应变状态。

2.2 Pt/BFO/LSCO/MgO 介电性能

室温条件下, Pt/BFO/LSCO/MgO 异质结构相对介电常数和介电损耗的频率依赖特性曲线如图 2a 所示。由图 2a 可知,随着频率的增加,不同偏压下的BFO 薄膜相对介电常数均呈逐渐减小的趋势,且在低频时减小得更快,而介电损耗则呈现先减小、后增加的趋势。经计算,从 100 Hz~8 MHz, BFO 薄膜相对介电常数减小率约为 38.9%,且在不同偏置电压下基本不变。一般认为,高频下薄膜内部具有较长弛豫时间类型的极化逐渐跟不上外加信号的变化,导致了介电常数的降低^[23]。从图 2a 可知,相对于介电常数的变化, Pt/BFO/LSCO/MgO 异质结构的介电损耗呈现先减小、后增大的趋势,在~100 kHz 时最小,为 0.016, 8 MHz 时增加到了 0.212,这主要是由于不同频率范围内电荷的弛豫机制所致。据报道,影响介电损耗的因素主要有电导损耗和介电响应损耗。其中,电导损耗包含 2 部分:介质层的漏电阻引起的损耗和电容上下电极的电阻引起的损耗^[24]。在低频范围 (<100 kHz),

漏导起主要作用,这会导致介电损耗随着频率的增大而减小;在高频范围 (>100 kHz),电介质在交变电场作用下,由于快速反复极化而产生的介电响应损耗主要起作用;在~100 kHz 的频率时,这 2 个弛豫过程之间将产生竞争,从而导致最小的介电损耗^[25]。不同温度下相对介电常数和介电损耗的频率依赖关系如图 2b 所示。可以看出,随温度增加,相对介电常数和介电损耗均增加,且在低频时增加更大,这主要归因于随温度的升高,可能是由于热激活电荷(空间电荷、电荷缺陷及缺陷复合物)的出现引起了较强的介电色散所致^[26]。

Pt/BFO/LSCO/MgO 异质结构电容器的 $C-V$ 曲线和 $J-V$ 曲线分别如图 2c、d 所示。可以看出, $C-V$ 曲线呈现出典型的蝶形特征,说明 BFO 薄膜具有很强的铁电性能。由于该异质结构的上下电极不对称,故正负矫顽电压存在明显差异,分别为~3.36 V 和~-1.12 V。很明显,负向势垒偏小,铁电畴易于极化反转,而正向势垒较大,故需要更大的电压实现极化反转。同理, $J-V$ 曲线也不对称,负电场下的漏电流明显大于正电场。在 5 V 时,正负电场下的漏电流密度分别为 8.16×10^{-4} 、 0.14 A/cm^2 ,相差近 2 个数量级。

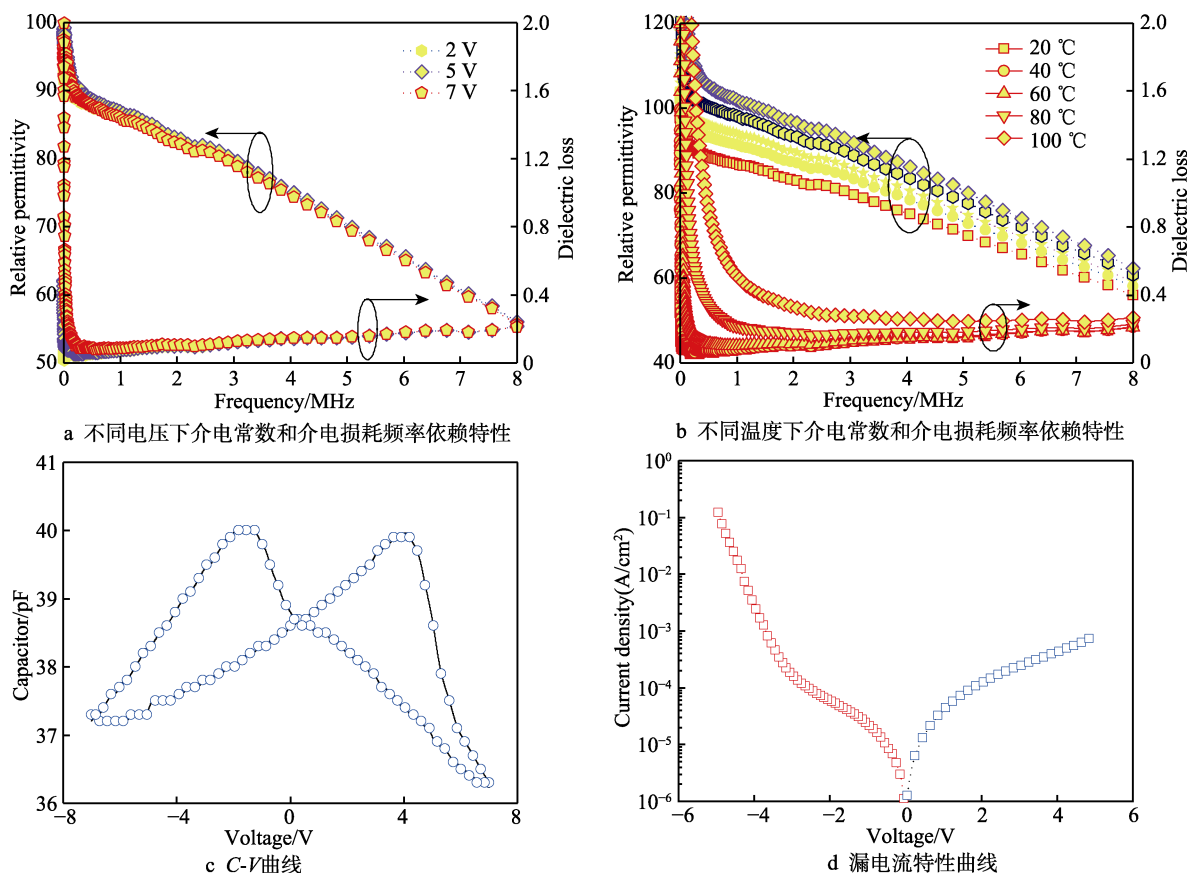


图 2 Pt/BFO/LSCO/MgO 异质结构的特性曲线

Fig.2 Characteristic curve of Pt/BFO/LSCO/MgO heterostructure: a) frequency dependence of dielectric constant and dielectric loss at different voltages; b) frequency dependence of dielectric constant and dielectric loss at different temperature; c) $C-V$ curve; d) leakage current characteristic curve

2.3 Pt/BFO/LSCO/MgO 光伏性能

Pt/BFO/LSCO/MgO 异质结构在-5 V 极化下的室温光伏性能如图 3a 所示。可以看出, 无光照环境下, BFO 薄膜几乎无电流产生, 而当用光强 250 mW/cm² 的紫光垂直照射薄膜表面时, 发现有明显的光伏效应产生, 其开路电压 (V_{OC}) 和短路电流 (J_{SC}) 分别为 0.32 V 和 0.21 mA/cm², 这与 Pei 等^[27]的研究结果 (V_{OC} 为~0.29 V, J_{SC} 为~0.26 mA/cm²) 相近。为进一步表征温度的影响, 图 3b 给出了不同测试温度 (20~100 °C) 和-5 V 极化下的 J - V 曲线。可以看出, 测试温度对 BFO 薄膜漏电流密度的影响较为显著。BFO 薄膜 V_{OC} 和 J_{SC} 随温度的变化情况如图 3c 所示, 结果表明, 当温度低于 80 °C 时, V_{OC} 缓慢减小, 但高于临界温度 80 °C 时, 快速减小。其 V_{OC} 由 0.32 V 减小为 0.30 V, 而 J_{SC} 随温度增加明显, 由 0.21 mA/cm² (20 °C) 增加到 0.96 mA/cm² (80 °C)。同样, 当高于临界温度 80 °C 则开始减小。该值优于目前领域内已报道的研究结果, 展现了更快光伏响应速度, 具体见表 2。BFO 薄膜在-5 V 极化后, 零偏压下短路电流随时间变化的光伏开关曲线如图 3d 所示。由图 3d 可知, 当无光照时, 短路电流为 0, 而用光强 250 mW/cm² 的紫光垂直照射后, 均有瞬时反应的光

电流产生, 且 J_{SC} 随着时间改变基本变化不大, 稳定性良好。当光照停止后, J_{SC} 瞬间减小到几乎为 0。因此, 可以看出, BFO 薄膜光响应很敏感。随着温度增加, J_{SC} 开始变大, 当达到 80 °C 后开始减小, 这一变化趋势与图 3b 相同, 主要可能归因于随温度的不断升高, 铁电畴本征反转增大, 导致铁电极化诱导的内建电场减小, 进而使 V_{OC} 随温度升高而减小。 J_{SC} 随温度升高先增大、后减小。在温度相对较低之时, 随着温度的逐渐升高, 本征激发产生的电子空穴对不断增加, 其影响超过了 V_{OC} 减小造成电流减小的情况, 使得 J_{SC} 随温度的增加而增大。随温度进一步增加, 晶格散射增大, 使其影响大于本征激发, 从而使电流减小^[28-29]。

2.4 Pt/BFO/LSCO 能带结构

Pt/BFO/LSCO/MgO 异质结构未极化时的能带如图 4a 所示。基于 BFO 薄膜上下电极的不对称性, 故存在不同的界面势垒, 这可从图 2c、d 有关 C - V 与 J - V 曲线的不对称性得到印证。据文献^[33-34]报道, LSCO、BFO 和 Pt 的功函数分别为 4.65、4.70、5.65 eV。可以看出, 因功函数差而产生的贯穿薄膜的静电场 (E_{in}) 为 1 eV。由于上电极 Pt 功函数大于下电极 LSCO, 所以 E_{in} 由 LSCO 指向 Pt。因此, 在光照射 BFO 薄膜

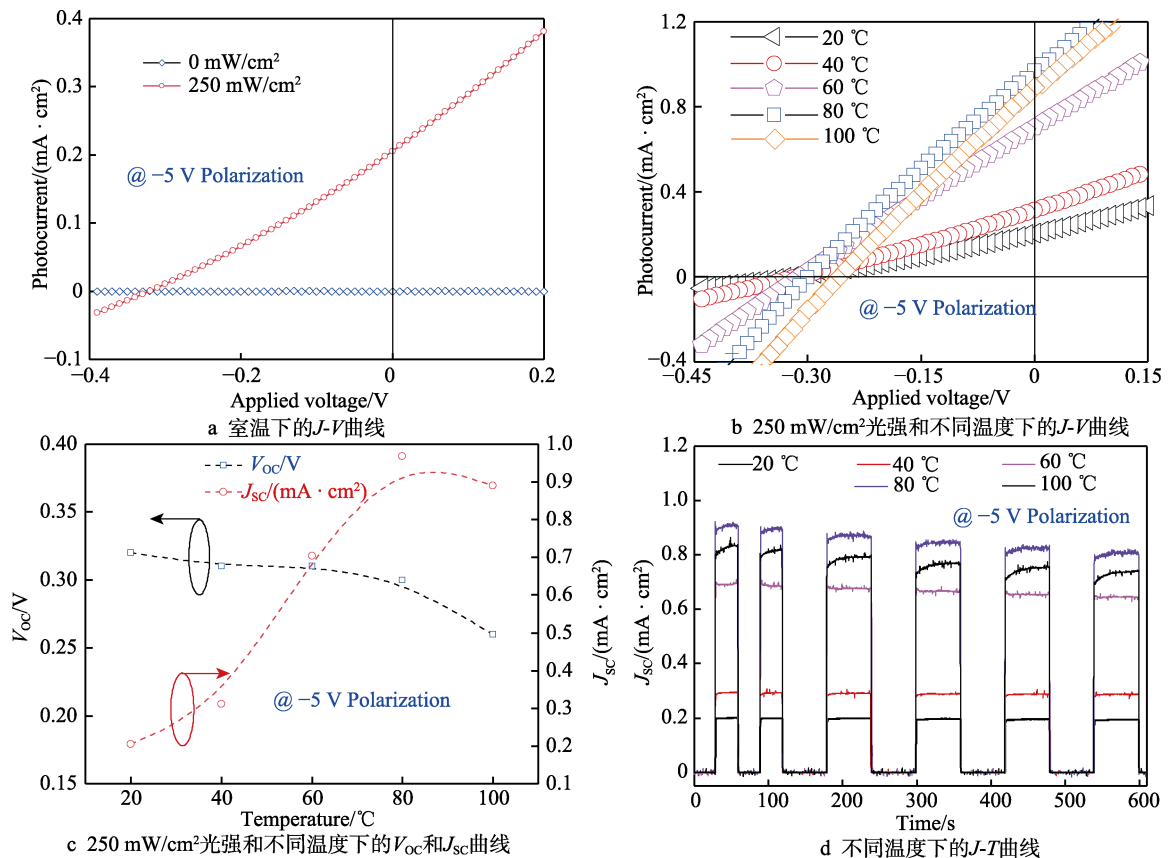


图 3 Pt/BFO/LSCO/MgO 异质结构光伏性能曲线

Fig.3 J - V curves, V_{OC} , J_{SC} curves, J - T curves of Pt/BFO/LSCO/MgO heterostructure under different conditions:

- a) J - V curve at room temperature; b) J - V curves at 250 mW/cm² light intensity and different temperature; c) V_{OC} and J_{SC} curves at 250 mW/cm² light intensity and different temperature; d) J - T curves at different temperature

表 2 BFO 基铁电薄膜的光伏性能对比
Tab.2 Comparison of photovoltaic properties in BFO based ferroelectric thin film

Materials	Methods	Temperatures/°C	V_{OC}/V	$J_{SC}/(mA \cdot cm^{-2})$	References
Pt/Bi _{0.925} Sm _{0.075} Fe _{0.95} Ni _{0.05} O ₃ /FTO	Sol-Gel	RT	0.45	0.113	[30]
FTO/Bi ₅ FeTi ₃ O ₁₅ /CuO/Au	Sol-Gel	RT	0.23	0.123	[31]
FTO/p-TiO ₂ /BFO/NiO/Au	Sol-Gel	RT	0.28	0.13	[32]
ITO/Bi _{0.98} Ca _{0.02} Fe _{0.95} Mn _{0.05} O ₃ /SrRuO ₃	PLD	RT	0.29	0.261	[27]
Pt/BiFeO ₃ /LaSrCoO ₃ /SrTiO ₃	Sputtering	RT	0.32	0.21	This paper
		80 °C	0.30	0.96	

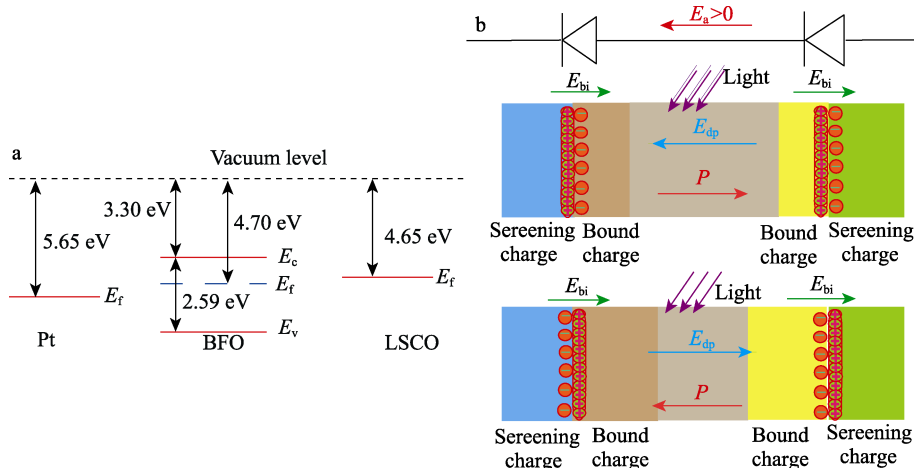


图 4 Pt/BFO/LSCO/MgO 异质结构的能带结构和加极化电场后能级变化
Fig.4 Pt/BFO/LSCO/MgO heterostructure: a) energy-band schematics for unpoled; b) energy level change after addition of polarized electric field

时, E_{in} 会分离光生载流子, 产生光伏效应。 E_{in} 的方向与负极化的方向相同, 在相同数值的正负电压下, 负方向有更大的漏电流。加极化场时 BFO 薄膜能级的变化情况如图 4b 所示。极化后会形成退极化场 (E_{dp}), 与 E_{in} 共同作用形成一个内建电场 (E_{bi}) 分离光生载流子。图 4b 中间图为负极化, 此时退极化方向左, 与 E_{in} 方向相反, $E_{bi}=E_{in}-E_{dp}$, 方向向右, 即由 LSCO 指向 Pt, 短路电流为正, 开路电压为负。图 4b 下部图为正极化, 退极化方向向右, 与 E_{in} 方向相同, E_{bi} 方向向右, 短路电流为正, 开路电压为负。光伏效应由极化产生的退极化场 E_{dp} 和异质结构 Pt/BFO/LSCO 电极不对称带来的内部电场 E_{in} 共同产生。 E_{in} 方向不变, E_{dp} 随极化而改变。因此, 可以选用合适的电极, 并进行适当极化, 以获得理想的 V_{OC} 和 J_{SC} 。

3 结论

本文基于(001)MgO 单晶作为衬底, 采用偏轴磁控溅射法外延 LSCO 薄膜作为底电极, 成功构架了 Pt/BFO/LSCO/MgO 异质结构铁电电容器。测试结果表明, BFO 薄膜具有结晶良好的外延钙钛矿结构、显著的铁电性和光伏特性, 尤其是在临界温度 80 °C 处, V_{OC} 和 J_{SC} 分别为 0.30 V 和 0.96 mA/cm², 表现出更快的光伏响应速度。因此, BFO 是一种性能优异的铁电光伏材料, 具有很大的潜在应用价值。

参考文献:

- [1] CHAI Zheng-jun, TAN Guo-qiang, YUE Zhong-wei, et al. Ferroelectric Properties of BiFeO₃ Thin Films by Sr/Gd/Mn/Co Multi-Doping[J]. Journal of Alloys and Compounds, 2018, 746: 677-687.
- [2] LIU Qing, ZHOU Yang, YOU Lu, et al. Enhanced Ferroelectric Photoelectrochemical Properties of Polycrystalline BiFeO₃ Film by Decorating with Ag Nanoparticles[J]. Applied Physics Letters, 2016, 108(2): 022902.
- [3] LEE H, KIM H S, GONG O Y, et al. Enhanced Ferroelectric Photovoltaic Effect in Semiconducting Single-Wall Carbon Nanotube/BiFeO₃ Heterostructures Enabled by Wide-Range Light Absorption and Efficient Charge Separation[J]. Journal of Materials Chemistry A, 2020, 8(20): 10377-10385.
- [4] YANG S Y, SEIDEL J, BYRNES S J, et al. Above-Bandgap Voltages from Ferroelectric Photovoltaic Devices [J]. Nature Nanotechnology, 2010, 5(2): 143-147.
- [5] TEH Y S, BHATTACHARYA K. Photovoltaic Effect in Multi-Domain Ferroelectric Perovskite Oxides[J]. Journal of Applied Physics, 2019, 125(6): 064103.
- [6] ZHANG Wei, YANG Ming-min, LIANG Xiao, et al. Piezotrain-Enhanced Photovoltaic Effects in BiFeO₃/La_{0.7}Sr_{0.3}MnO₃/PMN-PT Heterostructures[J]. Nano Energy, 2015, 18: 315-324.
- [7] SHARMA S, TOMAR M, KUMAR A, et al. Photovoltaic Effect in BiFeO₃/BaTiO₃ Multilayer Structure Fabricated

- by Chemical Solution Deposition Technique[J]. Journal of Physics and Chemistry of Solids, 2016, 93: 63-67.
- [8] XU Ze-dong, DENG Bei, HU Si-xia, et al. Strong Spin-Lattice Coupling in Tetragonal-Like BiFeO₃ Films with Thermal Expansion Anomalies[J]. Applied Physics Letters, 2020, 117(12): 122901.
- [9] CHRISTEN H M, NAM J H, KIM H S, et al. Stress-Induced R-M_A-M_C-T Symmetry Changes in BiFeO₃ Films [J]. Physical Review B, 2011, 83(14): 144107.
- [10] ZHOU Jin-ling, SANDO D, CHENG Xuan, et al. Tuning Phase Fractions and Leakage Properties of Chemical Solution Deposition-Derived Mixed-Phase BiFeO₃ Thin Films[J]. ACS Applied Electronic Materials, 2020, 2(12): 4099-4110.
- [11] SHIMIZU K, HOJO H, IKUHARA Y, et al. Enhanced Piezoelectric Response Due to Polarization Rotation in Cobalt-Substituted BiFeO₃ Epitaxial Thin Films[J]. Advanced Materials, 2016, 28(39): 8639-8644.
- [12] SCHLOM D G, CHEN Long-qing, EOM C B, et al. Strain Tuning of Ferroelectric Thin Films[J]. Annual Review of Materials Research, 2007, 37: 589-626.
- [13] MA Jing, HU Jia-mian, LI Zheng, et al. Recent Progress in Multiferroic Magnetoelectric Composites: From Bulk to Thin Films (Adv. Mater. 9/2011)[J]. Advanced Materials, 2011, 23(9): 1061.
- [14] SCHLOM D G, CHEN Long-qing, FENNIE C J, et al. Elastic Strain Engineering of Ferroic Oxides[J]. MRS Bulletin, 2014, 39(2): 118-130.
- [15] SÁNCHEZ-PÉREZ M, ANDRÉS J P, GONZÁLEZ J A, et al. Substrate-Induced Strain Effect on Structural and Magnetic Properties of La_{0.5}Sr_{0.5}CoO₃ Films[J]. Nanomaterials, 2021, 11(3): 781.
- [16] LIU B T, CHEN J E, SUN J, et al. Oxygen Vacancy as Fatigue Evidence of La_{0.5}Sr_{0.5}CoO₃/PbZr_{0.4}Ti_{0.6}O₃/La_{0.5}Sr_{0.5}CoO₃ Capacitors[J]. EPL (Europhysics Letters), 2010, 91(6): 67011.
- [17] FU Y J, XIA F J, JIA Y L, et al. Bipolar Resistive Switching Behavior of La_{0.5}Sr_{0.5}CoO_{3- Σ} Films for Nonvolatile Memory Applications[J]. Applied Physics Letters, 2014, 104(22): 223505.
- [18] XU Huang, SHI jian jun, LI xiao yun, et al. Oriented (100) Electrical Property of BiFeO₃/La_{0.7}Sr_{0.3}MnO₃ Multilayered Thin Films[J]. Applied Mechanics and Materials, 2013, 378: 270-274.
- [19] GAZQUEZ J, BOSE S, SHARMA M, et al. Lattice Mismatch Accommodation via Oxygen Vacancy Ordering in Epitaxial La_{0.5}Sr_{0.5}CoO_{3- δ} Thin Films[J]. APL Materials, 2013, 1(1): 012105.
- [20] SHARMA A, BAN Z G, ALPAY S P, et al. Pyroelectric Response of Ferroelectric Thin Films[J]. Journal of Applied Physics, 2004, 95(7): 3618-3625.
- [21] SINGH S K, ISHIWARA H, MARUYAMA K. Enhanced Polarization and Reduced Leakage Current in BiFeO₃ Thin Films Fabricated by Chemical Solution Deposition [J]. Journal of Applied Physics, 2006, 100(6): 064102.
- [22] LU Sheng-bo, XU Zheng-kui. Internal Residual Stress Studies and Enhanced Dielectric Properties in La_{0.7}Sr_{0.3}CoO₃ Buffered (Ba, Sr)TiO₃ Thin Films[J]. Journal of Applied Physics, 2009, 106(6): 064107.
- [23] MOHARANA S, MAHALING R N. Preparation and Properties of Benzoxazine (BA) Based BiFeO₃-Poly(vinylidene fluoride) (PVDF) Composites: Enhanced Dielectric Constant and Suppressed Loss[J]. Polymer-Plastics Technology and Materials, 2021, 60(10): 1122-1134.
- [24] CHEN X Q, QI H Y, QI Y J, et al. Ferroelectric and Dielectric Properties of Bismuth Neodymium Titanate Ceramics Prepared Using Sol-Gel Derived Fine Powders [J]. Physics Letters A, 2005, 346(1/2/3): 204-208.
- [25] ZHU Han-fei, MA Hong-fang, ZHAO Yu-yao. Role of Rapid and Slow Cooling on Leakage Mechanism and Ferroelectric Polarization of Sputtered Epitaxial BiFeO₃ Thin Films[J]. Vacuum, 2019, 163: 312-316.
- [26] SINGH G, BHASKER H P, YADAV R P, et al. Dielectric, Magnetic and Magneto-Dielectric Properties of (La, Co) Co-Doped BiFeO₃[J]. Physica Scripta, 2019, 94(12): 125805.
- [27] PEI Wei-jie, CHEN Jian, YOU Di, et al. Enhanced Photovoltaic Effect in Ca and Mn Co-Doped BiFeO₃ Epitaxial Thin Films[J]. Applied Surface Science, 2020, 530: 147194.
- [28] YUAN Guo-liang, CHEN Jiang-peng, XIA Hui, et al. Ferroelectric Domain Evolution with Temperature in BaTiO₃ Film on (001) SrTiO₃ Substrate[J]. Applied Physics Letters, 2013, 103(6): 062903.
- [29] 何东昱, 刘玉欣. 0.8PbTiO₃-0.2Bi(Mg_{0.5}Ti_{0.5})O₃ 铁电薄膜 90°分步畴转与温度效应[J]. 金属学报, 2019, 55(3): 325-331.
- HE Dong-yu, LIU Yu-xin. PFM Study of the 90° Step-by-Step Domain Switching and the Temperature Effect in 0.8PbTiO₃-0.2Bi(Mg_{0.5}Ti_{0.5})O₃ Ferroelectric Thin Film[J]. Acta Metallurgica Sinica, 2019, 55(3): 325-331.
- [30] ZHANG Lin-xing, CHEN Jun, CAO Jiang-li, et al. Large Resistive Switching and Switchable Photovoltaic Response in Ferroelectric Doped BiFeO₃-Based Thin Films by Chemical Solution Deposition[J]. Journal of Materials Chemistry C, 2015, 3(18): 4706-4712.
- [31] ZHU Ming-sai, ZHENG Hai-wu, ZHANG Ju, et al. Polarization Dependent Ferroelectric Photovoltaic Effects in BFTO/CuO Thin Films[J]. Applied Physics Letters, 2017, 111(3): 032901.
- [32] WANG Ling-fei, MA He, CHANG Lei, et al. Ferroelectric BiFeO₃ as an Oxide Dye in Highly Tunable Mesoporous All-Oxide Photovoltaic Heterojunctions[J]. Small, 2017, 13(1): 1602355.
- [33] NAGARAJ B, AGGARWAL S, RAMESH R. Influence of Contact Electrodes on Leakage Characteristics in Ferroelectric Thin Films[J]. Journal of Applied Physics, 2001, 90(1): 375-382.
- [34] YIN Li, MI Wen-bo. Progress in BiFeO₃-Based Heterostructures: Materials, Properties and Applications[J]. Nanoscale, 2020, 12(2): 477-523.